PCCP

ROYAL SOCIETY OF CHEMISTRY

ARTICLE TYPE

Cite this: DOI: 10.1039/xxxxxxxxxx

Influence of Cu Adatoms on the Molecular Assembling of 4,4'-Bipyridine on Cu(111)

M.-A. Dubois,[a] O. Guillermet,[b,c], S. Gauthier[b], G. Zhan[d], Y. Makoudi[d], F. Palmino[d], X. Bouju[b] and A. Rochefort*‡[a]

Received Date
Accepted Date

DOI: 10.1039/xxxxxxxxxx

www.rsc.org/journalname

The formation of highly organized structures based on two ligands with pyridyl functionalities, 4,4'-bipyridine (BPY) and 1,4-di(4,4"-pyridyl) benzene (BPYB)), and Cu adatoms on the Cu(111) surface has been studied with low temperature and variable temperature scanning tunneling microscopy (STM) and first-principle calculations. We are showing that the formation of a highly organized adlayer built from adatom-molecule and molecule-molecule units strongly depends on the amount of mobile Cu atoms on the surface. While a high concentration of Cu adatoms (high adatom/BPY ratio, $\geq$ 1) leads systematically to the formation of organometallic nanolines, the absence of them (low adatom/BPY ratio, $\approx$ 0) gives compact self-assembled molecular network, and more specifically hydrogen-bond networks (HBN) with BPY molecules organized in a T-shaped fashion. Alternatively, an intermediate concentration of Cu adatoms (0 $<$ adatom/BPY $<$ 1) allows the formation of a well-organized and compact structure where both organometallic and HBN components coexist. Although STM images cannot clearly reveal the presence of Cu adatom within the organometallic moiety, the bonding of BPY to a single or two Cu adatoms can be clearly identified by tunneling spectroscopy (STS), and is supported by Density Functional Theory (DFT) results. Additional STM simulations suggest that the relative position of the Cu adatom with respect to organic ligands just above has a significant impact on its detection by STM. This study exemplifies the prominent role of metallic adatoms on the formation of complex organometallic network and should open more rational practices to optimize the formation of those supramolecular networks.

1 Introduction

The rational design of supramolecular networks on metallic surfaces based on the molecular interactions between building blocks (molecules, atoms) that establish highly directional bonding can now be performed for a large class of species.[1,2] Although the major progress in the preparation of controlled molecular networks during the last decade, there are still open fundamental issues that remain difficult to predict. Among them, the understanding of magnitude of molecule-molecule and molecule-surface interactions is an example of the most central challenges that need to be accurately addressed in order to anticipate any supramolecular networks. In the situations where the molecule-surface interactions are very strong, the metallic surface plays a central role by imposing a rigid geometry to the molecular adlayers through its crystal lattice[3], but may also contain numerous amount of structural defects when the lattices do not match, or more subtle, may lead to organization on a much longer range for the molecular species.[4,5] In contrast, when the molecule-molecule interactions are stronger, the assembling process depends essentially on the ability of the molecules to establish strong directional bonds to create a dense molecular network.[6,7]

A different route to generate supramolecular networks uses atomic metal species to bind molecules in a highly organized fashion.[1,8] Metal surface atoms mostly originate from step edges of single crystals where they rapidly diffuse, or they can also be evaporated from an external metal source to the surface.[8] In these organometallic complexes, metal adatoms are highly reactive toward organic species, but their affinity with the metal surface remains quite high. Thus, very stable organometallic complexes are formed where the metal atom generally sits on a high

[a] *Département de génie physique et Regroupement québécois sur les matériaux de pointe (RQMP), Polytechnique Montréal, Montréal, Québec, H3C 3A7, Canada.*
[b] *Centre d'élaboration de matériaux et d'études structurales, CEMES-CNRS, UPR 8011, Nanosciences Group, 29 rue Jeanne Marvig, F-31055 Toulouse, France.*
[c] *Université de Toulouse, UPS, 29 rue J. Marvig, F-31055 Toulouse, France.*
[d] *Institut FEMTO-ST, Université Bourgogne Franche-Comté, CNRS, 15B Avenue des Montboucons, F-25030 Besançon Cedex, France.*
‡ E-mail : alain.rochefort@polymtl.ca.

coordination adsorption site.[9–16] Hence, the building blocks in these networks are mainly symmetric organometallic complexes built from the few organic ligands bonded to one or more metal atoms, and are localized on the preferential adsorption sites of the surface. In this case, the concentration of metal surface atoms has a direct impact on the nature and the dimension of the organized regions, and we may expect to observe a mixture of adsorbed phases at high ligand/metal ratios. Interestingly, the co-deposition of iron atoms and an acidic molecule on a bulk insulator generates a metal-organic coordination network according to the order of deposition, that is to say only if molecules are deposited first and subsequently the metal atoms.[17]

In this paper, two molecules with pyridyl moieties were chosen to study the influence of the adatom concentration on the structure of the molecular assembly. Indeed, in absence of surface adatoms, a hydrogen network is exclusively formed, while organometallic nanolines are mostly formed at high adatom/BPY ratio, and a mixture of the two previous cases are formed for intermediate adatom/BPY ratio. STS experiments were successful to reveal the presence of adatoms within the nanolines although they cannot be clearly seen in STM images. Our DFT calculations and STM simulations support the presence of such adatoms, and bring some explanations on the difficulty in observing them on STM images.

2 Experimental Details

The scanning tunneling microscopy (STM) images were recorded with a commercial low temperature and a variable temperature STM from Scienta Omicron. STM images were acquired in a constant-current mode at 110 K, 77 K or 4 K. The Cu(111) and Ag(111) samples were cleaned by repeated Ar sputtering followed by annealing at 750 K. The 4,4'-bipyridine (BPY) molecules and 1,4-di(4,4"-pyridyl) benzene (BPYB) molecules have been evaporated in ultra-high vacuum from powder kept at room temperature (BPY) or by a thermal annealing (BPYB). The length of BPY and BPYB molecules are respectively of 0.716 nm and 1.151 nm (see Fig. 1). At room temperature, BPY is known to have a relatively high vapor pressure (10^{-5} mbar) compared to the UHV conditions (10^{-11} mbar). Consequently, BPY powder was placed in an adjacent pumped chamber, and a fine adjustment of pumping speed and valve opening was necessary to introduce a 10^{-8} to 10^{-7} mbar partial pressure in the preparation chamber.

3 Computational Methodology

The electronic structure calculations were performed within Density Functional Theory (DFT) methods included in the NwChem package.[18] The molecular structures were fully optimized without any symmetry constraints with a quasi-Newton technique until the gradient convergence factor was lower than 10^{-5} Hartree/Bohr. In order to accurately evaluate the dissociation energies of metal-ligand bonds, we have used extended basis sets, PBE0 exchange-correlation functionals and van der Waals (vdW) corrections.[19]

The STM simulations were carried out with our in-house DyFlex software[20] that is a dynamical version of the Flex-STM code[21] developed in our group. For the present study, we used extended Hückel Hamiltonians included in the YaeHmop package[22] in conjunction with the Tersoff-Hamann (TH) level of theory to produce all simulated STM images. Images were generated at constant height (7.5 Å) from the surface, and different positive and negative bias were considered. Notice that the TH approximation is relevant for the flat molecular system considered here[23] without the use of more sophisticated methods like ESQC for instance that includes explicitly the atomic structure of the tip.[24]

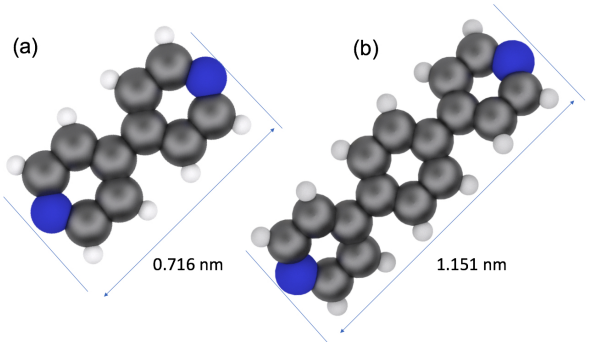

Fig. 1 (a) Representation of 4,4'-bipyridine (BPY) and (b) 1,4-di(4,4"-pyridyl) benzene (BPYB) molecules.

4 Results and Discussion

4.1 Room temperature adsorption

We first start our experiment by introducing 6 L of 4,4'-bipyridine (BPY) at room temperature on the Cu(111) surface. Figure 2(a) shows a STM image of the self-assembled structure with ladder-like patterns. A BPY molecule is represented by a single bright protrusion. Based on the STM image of the substrate (not shown), we note that the molecular lines are turned by $12^\circ \pm 3^\circ$ from Cu(111) low index directions, and only a small and alternate deviation of molecular axis is observed with an average distance of 10.5 ± 0.3 Å between molecules. A closer examination reveals an alternate proximity of the ladder-like structure with one side of the lines (see Fig. 2(b)) in agreement with an inversion center. This assumption involves a molecular pairing for the ladder and line structures with non-equivalent adsorption sites. In fact, we observe a series of staircase structures that are sometimes separated by a single continuous bright line.

The STM image profiles of these structures along two different paths (A, B) are presented in Fig. 2(c). It is clear that both paths give rise to regular distributions of STM contrasts where the ladder-like structures are paired (line B) with one shorter than the other, as revealed by the black scale lines given in that figure. The profile of these paired structures (line B) remains tightly linked to the pattern observed in profile A. Nevertheless, the width of the features in line B are narrower than those of line A, suggesting that the BPY in line B are perpendicular to the ones in line A. The average distance between the bright spots along line A is 10.5 ± 0.3 Å, and for the line B, we measured 12.5 ± 0.3 Å and 8.6 ± 0.3 Å for respectively, the long and short features. These results reveal that the adsorption of BPY is strongly directed by the Cu(111) lattice.

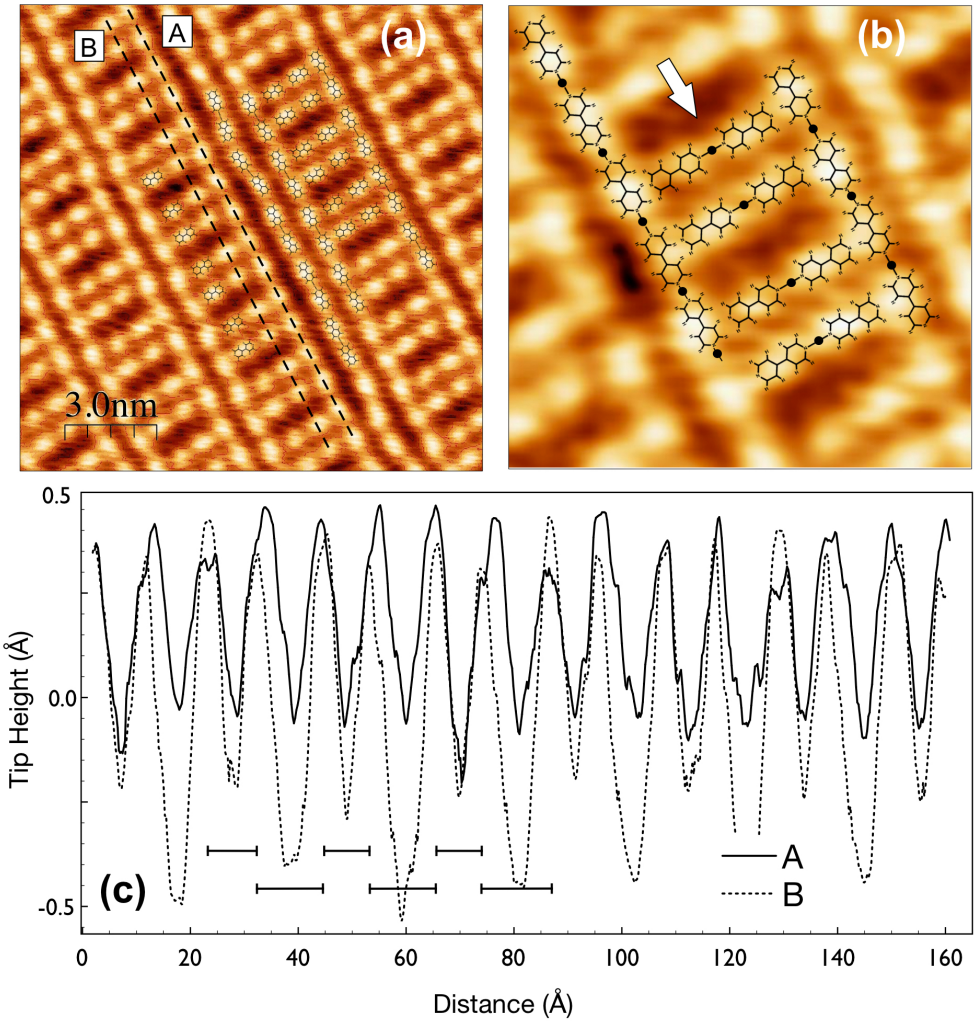

Fig. 2 (a), (b) STM images recorded at 4 K, (c) STM profiles along line A and B. For line B, one observes two alternate categories of distances between maxima as indicated by the horizontal bars. ($V_s = +0.1$ V)

According to previous studies on similar systems, the adsorption of the BPY molecules along a straight line should be repulsive except when a Cu adatom is bridging two pyridine units.[26,27] We performed DFT calculations (6-31G**/PBE0+vdW) that support that two BPY molecules do not form a stable complex when aligned into a straight line, but BPY becomes weakly bonded by 0.10 eV when the molecules adopt a T-shape. In fact, the number of mobile Cu adatoms on the Cu(111) surface should be significantly high at room temperature,[8] and more especially near steps edges. Admitting the presence of Cu adatoms, the formation of a nanoline along the A profile should then involve a repetitive -(Cu-BPY)- organometallic unit while the transverse BPY molecules cannot be fully coordinated to Cu adatoms since otherwise it would have formed a straight nanoline. In these rungs, two BPY molecules are bonded to a single Cu adatom in the center while the molecular extremities are weakly bonded to BPY in the nanolines in a T-shaped configuration. Furthermore, we are forced to admit that most STM images reported in the literature about Cu or Au adatom-molecule complexes,[1,8,9,11,16,25–27] including the present results, cannot hardly support the presence or absence of Cu atoms in this ladder-like assembly of BPY on Cu(111). Even the higher resolution STM image shown in Fig. 2(b) is not convincingly supporting such Cu adatom participation to the nanolines along the pathway A, nor in the middle region of the rungs features (identified by the large white arrow).

A series of differential conductance spectroscopy (STS) measurements were performed in the nanolines and rungs region to compare the electronic properties of the BPY moiety. In comparison, we have also performed DFT calculations to compare the electronic structure of an isolated BPY molecule and a BPY molecule bonded to a single or to two Cu dimers. The STS and DFT results are summarized in Fig. 3. The STS spectrum of an isolated BPY monomer shows only a tiny shoulder at +1.6 V, the BPY molecules from the rungs show a clear peak at +1.6 V while the BPY species within the nanoline structure give a peak at +1.3 V. DFT results cannot be clearer to describe the origin of those peaks. The state at +1.6 V originates from the bonding of BPY to a single Cu atom, involving the mixing of LUMO (BPY) and d-orbitals of Cu. The peak at +1.3 V corresponds to the bonding of BPY to two Cu atoms, also involving LUMO of BPY and d-orbitals of Cu. STS and DFT results strongly support that nanolines are formed from a series of (Cu-BPY) units, while the ladders are made of BPY-Cu-BPY isolated units. A second series of DFT calculations were performed to investigate the stability of Cu-BPY complexes. Table 1 indicates that once a Cu-BPY bond is formed, it becomes more energetically favorable for this species to bind an additional BPY molecule than a second Cu atom. This stability then suggests that a $Cu(BPY)_2$ complex could represent a realistic building unit. The significant interaction energy for the formation of a Cu-BPY$\cdots$Cu complex also supports the formation of one dimensional nanostructures containing chains of repetitive (Cu-BPY) units.

From the size and intensities of the different STM features observed and the results of DFT calculations, we propose the model shown in Fig. 4. The geometry of the BPY-Cu fragment used in that figure were taken from our DFT calculations. According to the 12° misorientation of the molecular lines and to an

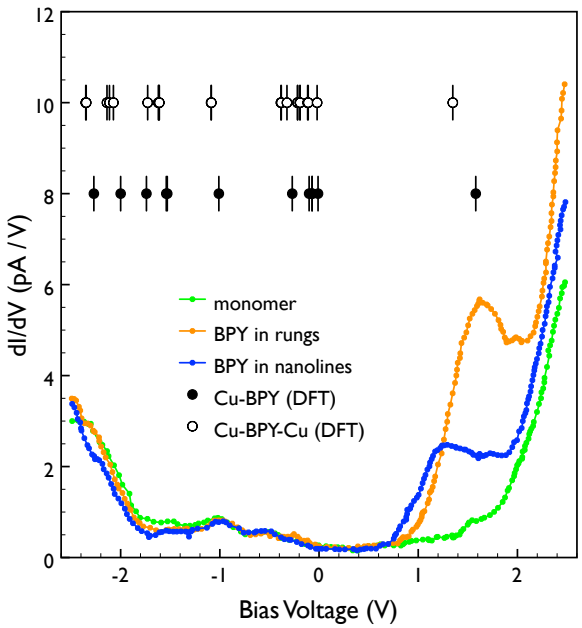

Fig. 3 Differential conductance (dI/dV) spectra of BPY as isolated on the surface (red), in the nanoline (blue) and in the rungs (green) regions. The circles are the position of energy levels calculated from DFT for Cu-BPY (filled) and Cu-BPY-Cu (opened) complexes.

Table 1 Calculated interaction energies (eV) of Cu-BPY complexes

level	Cu$\cdots$BPY	Cu-BPY$\cdots$Cu	BPY-Cu$\cdots$BPY
6-31G/PBE0+vdW	−3.00	−2.74	−2.86
6-31G**/PBE0+vdW	−1.67	−1.49	−2.65
6-31^{++}G**/PBE0+vdW	−2.06	−1.89	−2.39

inversion center, the primitive unit mesh would correspond to a $[13\times-5,\ 2\times7]$ to allows each Cu atoms to remain on the same hollow adsorption site. In agreement with this lattice unit, the distance between features in lines A (10.5 Å) fits the $[2\times7]$ length (20.87 Å $\approx 2\times$ 10.45 Å) and the measurements along line B correspond to the distances measured within the rungs arrangement (8.92 Å and 12.29 Å). Fig. 4 shows a domain of the ladder-like structure with the sidelines built from (BPY-Cu) units where the Cu adatoms are systematically located on three-fold sites of the Cu(111) surface. The more central rungs features are BPY-Cu-BPY units where the Cu atom is sitting on a three-fold site, and the terminal pyridine groups are establishing a T-shaped interaction with a BPY in the sidelines. In order to maximize both Cu-surface and T-shaped complexes, one central rung features over two is displaced to finally form a pairwise structure. This model matches also very well the STM image recorded at 4 K in terms of distances between the different STM features.

4.2 Influence of Cu adatoms concentration

The model of BPY adsorbed on Cu(111) in Fig. 4 could be quite satisfying, but the presence or absence of Cu adatoms in the

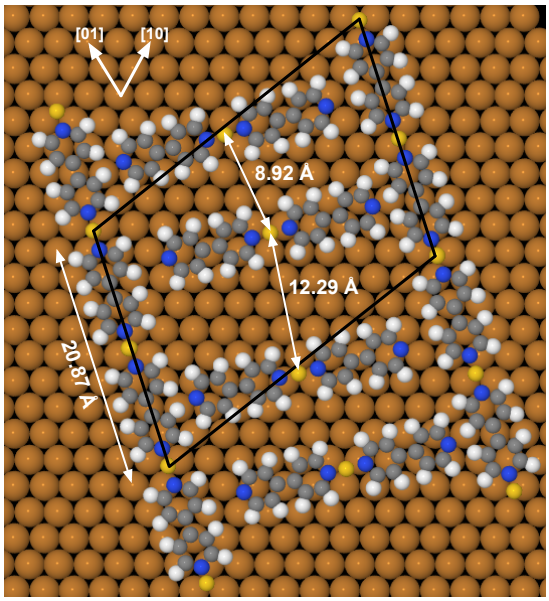

Fig. 4 Top view of a molecular model for the self-assembled layer of BPY on Cu(111) when the adatom/BPY ratio is between 0 and 1. The position of Cu adatoms underneath the BPY layer on Cu(111).

assembled layer still remains an open question that cannot be clearly evidenced in terms of STM contrasts. The most intriguing question remains the role of adatoms on the more central feature of the ladder-like structure. In order to clarify this point, we have carried out an adsorption of BPY at room temperature on Ag(111) where mobile adatoms do not specifically bind to pyridine moieties. As shown in Fig. 5, BPY molecules form exclusively large domains where the BPY units are organized into a T-shaped fashion. This confirms that adatoms are needed to form lines. Furthermore this observation confirms the selective character of the Cu-pyridine interaction (relative to Ag-pyridine), as observed experimentally[25] and supported by DFT calculations[28]. In addition, STS experiments on this BPY/Ag(111) overlayer reveal a peak at $+1.74$ eV. In agreement with Fig. 3, this peak can be associated to a weakly bonded BPY specie on the Ag(111) surface. It is also worth noting the absence of BPY molecules well-aligned into a straight isolated line.

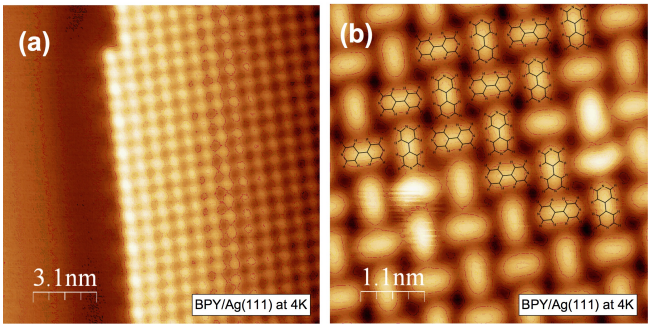

Fig. 5 STM images of BPY/Ag(111) recorded at 4 K with different resolutions. ($V_s = +0.1$ V)

The existence of weakly bonded T-shaped structure on Cu(111) should be easily demonstrated simply by showing their disappearance upon a moderate heating of the sample. After heating the Cu(111) sample at 350 K, the STM image shown in Fig. 6(a) indicates the absence of any organization of BPY into a ladder-like structure but instead it shows the presence of continuous lines of Cu-BPY that essentially begin and finish near a step edge, and that surprisingly do not cross each others. In addition, the higher resolution STM image in Fig. 6(b) shows that the composition of the Cu-BPY lines appears quite regular on the surface. Again, STM image does not reveal more specific features related to the presence of Cu adatoms, but since we observe the formation of 1D structure of BPY, we may assume the presence of Cu atoms in these chains.[26]

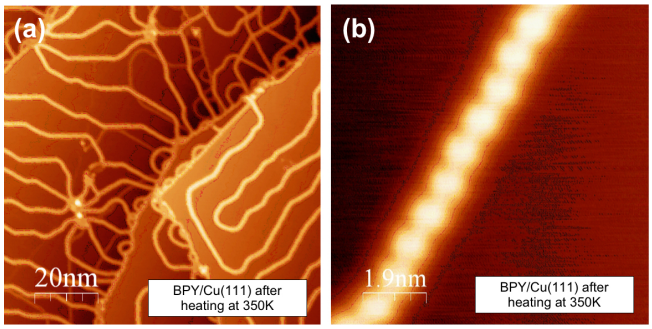

Fig. 6 STM images of BPY/Cu(111) recorded at 4 K with different resolutions after heating at 350 K. ((a) $V_s = +2.0$ V, $I_t = 2$ pA (b) $V_s = +0.05$ V, $I_t = 1$ pA)

The influence of copper adatoms density on the T-shape or nanolines formation was confirmed by depositing BPY on a sample kept at low temperature. Since our experimental setup is not equipped with a variable temperature sample older, Cu(111) was quickly removed from the microscope at 77 K and exposed to a 10^{-8} mbar of BPY for 20 sec. STM image in Fig. 7 shows the formation of mixed wires made of an alternation of T-shape assembly and small portions of nanolines. Furthermore, isolated BPY monomers can be observed on the surface. STS spectroscopies obtained on T-shape molecules or on the nanolines are similar to the ones obtained on the monolayer. Monomers only exhibit a small peak at $+1.6$ V, denoting the requirement of adjacent molecules or adatoms for the establishment of the observed states. The formation of BPY-Cu assembly requires the diffusion of copper and/or BPY. In the present case, we evaluate the deposition temperature by checking the monomers diffusion by STM, which occur between 120 and 130 K.

Another way to change the adatom/molecule ratio in to extend the molecule by inserting a central benzene ring to form 1,4-di(4',4"-pyridyl)benzene (BPYB), while keeping the pyridine groups (Fig. 1b). Indeed, for a same molecular nanoline length the second molecule (BPYB) needs fewer copper adatoms, and hence gives a lower adatom/molecule ratio. Moreover, as we are deposing the two molecules under the same conditions, the adatom/molecule ratio is greater in the case of the longer molecule (BPYB). Whatever the coverage of the BPYB molecules, we obtained structures in the form of nanolines. These nanolines are more or less spaced according to this rate. The STM image in Fig. 8 is an example for a relatively high BPYB recovery rate.

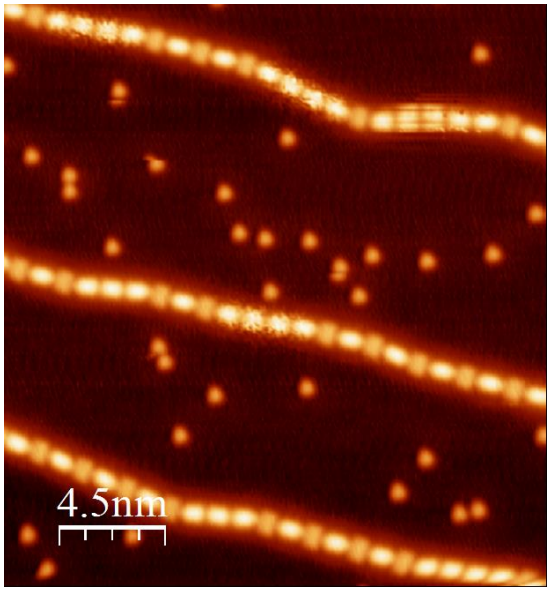

Fig. 7 STM image recorded at 77 K after a BPY deposition on Cu(111) kept below 130 K ($V_s = +1$ V, $I_t = 5$ pA).

As for the case of BPY, we can easily recognized the molecules; a bright spot corresponds to a BPYB molecule well-spaced by copper adatom. Based on these results, we can better understand the T-shaped structure observed for the smaller BPY molecule. Indeed, in the case of BPY molecule we need a higher adatom/BPY ratio to form lines with similar length. When they are depleted, these molecules prefer to rank between the lines through hydrogen bonding.

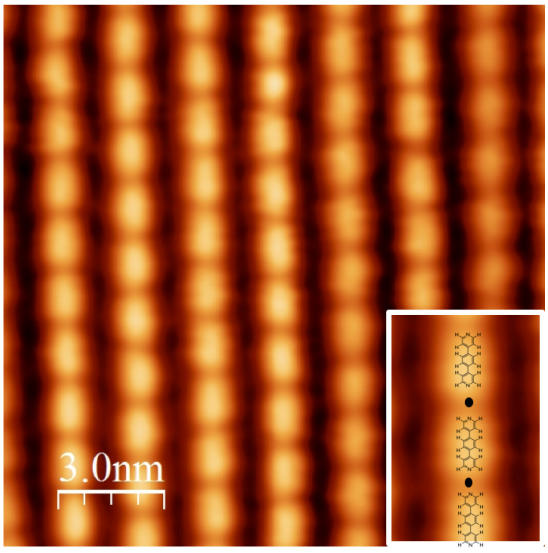

Fig. 8 STM image of BPYB/Cu(111) recorded at 110 K. ($V_s = -1.9$ V, $I_t = 10$ pA).

4.3 STM signature of Cu adatoms

Finally, we want to discuss the fact that STM images cannot clearly reveal the presence of Cu adatoms within surface complexes while STS measurements indicate their contribution to the bonding with BPY on the Cu(111) surface. Since Cu adatoms are more probably adsorbed in three-fold sites of the Cu(111) surface where they would occupy a bulk-like site, we may presume that Cu adatoms could be below the adsorbed BPY layer. From this premise, we have investigated two different scenarios for Cu adatoms to give a negligible contribution to STM images. This was performed with the help of STM simulations using our DyFlex software.[20,21]

First, Fig. 9 compares the variation of the STM contrasts from a simple BPY-Cu-BPY complex on a Cu(111) surface where a Cu adatom is located at $h_e = 1.70$ Å over a hollow site of the Cu(111) surface while the two BPY molecules are at 3.0 Å ($h_e + 1.30$ Å). As shown in the upper STM images in Fig. 9, the STM simulations using such arrangement reproduce the main STM experimental features in which the Cu adatoms weakly contribute to the tunneling current. To evaluate the influence of the Cu adatom on STM features, we considered the two displacements shown in the top part in Fig. 9: (a) a lift-off of the Cu adatom toward BPY, and (b) an increasing separation between the two BPY molecules. In each cases, we show the calculated tunneling current on a high resolution grid (0.3 Å); pixel by pixel on the left side and averaged over the pixels contained within a radius of 2 Å on the right side that emulates a more realistic STM apex. Figure 9(a) shows that the height of the Cu adatom has a drastic effect on the STM contrasts that supports the model proposed in Fig. 4 where the Cu adatoms are located underneath the BPY molecules on the Cu(111) surface. Otherwise, the contribution of adatoms is rapidly dominating the STM signal as the Cu adatoms become closer to the BPY layer. In addition, Fig. 9(b) shows the influence of the distance between the BPY molecules, that increases from 2.6 Å ($d_e = 0.0$ Å) to 3.4 Å ($d_e + 0.8$ Å). This increasing spacing between BPY molecules decreases the overlap between Cu adatom and the BPY molecules. Hence, the charge density on Cu adatom increases as well as the tunneling current over that specie. The trends observed in these STM simulations, combined with the experimental observations, suggest that the Cu adatom is more probably tightly bonded to BPY, and is located underneath the BPY units. Beyond our STM simulations, different STM works performed on a single adatom species also suggest that STM contrasts strongly depends on the charge state of the adsorbed adatom.[31,32]

5 Conclusions

We have studied the influence of Cu adatoms on the formation of an organized overlayer where organometallic complexes and molecular assemblies can be formed on the Cu(111) surface. High concentration of mobile Cu adatoms favors the formation of continuous nanolines made of (Cu-BPY) units. Intermediate Cu adatom concentration leads to the formation of ladder-like arrangement where the (Cu-BPY) units form the sidelines and individual molecular BPY-Cu-BPY units are connecting both sidelines through hydrogen bonding. In absence of Cu adatom, BPY molecules self-assembled into large domain where the BPY units are weakly bonded into a T-shaped fashion. Although STM experiments were not convincingly demonstrated the presence of Cu adatoms into the adsorbed layer, their signature was clearly ob-

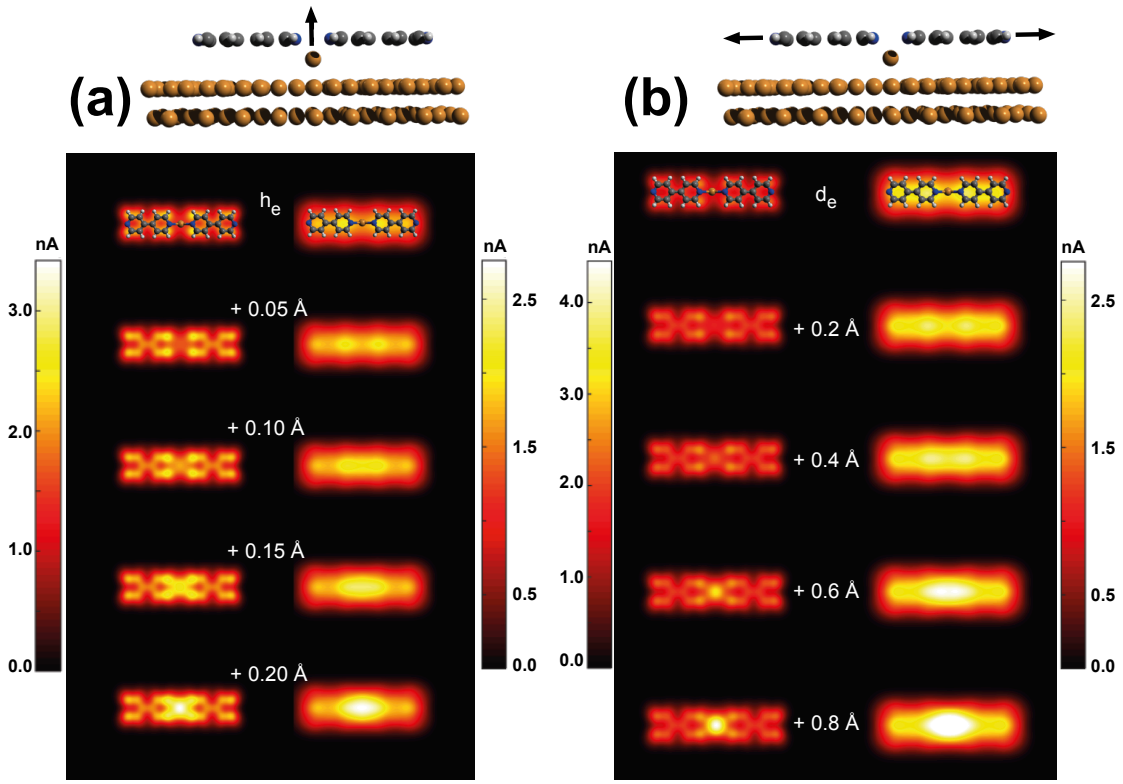

Fig. 9 Simulated STM images of Cu-BPY complexes on Cu(111) as a function of (a) the relative position of the Cu adatom with respect to an equilibrium position h_e, and (b) the relative distance between BPY groups with respect to an equilibrium position d_e. STM images are shown without any convolution on the left side, and with a radial convolution of 2 Å on the right side. STM images were simulated at constant height, $V_s = +1.5$ V.

served with the help of differential conductance spectroscopy and explained by DFT and STM simulations.

6 Acknowledgement

This work was supported by the Natural Sciences and Engineering Research Council of Canada (NSERC). A.R. is highly grateful to the Programme Investissements d'Avenir under the program ANR-11-IDEX-0002-02, reference ANR-10-LABX-0037-NEXT for financial support. This work would not be possible without the computational resources provided by Calcul Québec and Compute Canada. F.P., Y.M. and G.Z. acknowledge the financial support from the French National Research Agency through contract ORGANIâĂŹSO (ANR-15-CE09-0017) and from the Pays de Montbéliard Agglomération. We would also like to thank Dr. F. Chérioux for fruitful discussions.

References

1 J. V. Barth, G. Costantini and K. Kern, Engineering Atomic and Molecular Nanostructures at Surfaces, *Nature* 2005, **437**, 671-679.

2 X. Bouju, C. Mattioli, G. Franc, A. Pujol and A. Gourdon, Bicomponent Supramolecular Architectures at the Vacuum-Solid Interface, *Chem. Rev.* 2017 **117**, 1407-1444.

3 J.A.A. Elemans, S. Lei and S. De Feyter, Molecular and Supramolecular Networks on Surfaces: From Two-Dimensional Crystal Engineering to Reactivity, *Angew. Chem. Int. Ed.* 2009, **48**, 7298-7332.

4 A. Kühnle, Self-assembly of organic molecules at metal surfaces, *Current Opinion in Colloid & Interface Science* 2009, **14**, 157-168.

5 G. Hong, Q.-H. Wu, J. Ren, C. Wang, W. Zhang and S.-T. Lee, Recent progress in organic molecule/graphene interfaces, *Nano Today* 2013, **8**, 388-402.

6 A. Ulman, Formation and Structure of Self-Assembled Monolayers, *Chem. Rev.* 1996, **96**, 1533-1554.

7 T. Kudernac, S. Lei, J. A. A. W. Elemans and S. De Feyter, Two-Dimensional Supramolecular Self-Assembly: Nanoporous Networks on Surfaces, *Chem. Soc. Rev.* 2009, **38**, 402-421.

8 N. Lin, S. Stepanow, M. Ruben and J. V. Barth, Surface-Confined Supramolecular Coordination Chemistry, *Topics in Current Chemistry* 2009, **287**, 1-44.

9 A. Dmitriev, H. Spillmann, N. Lin, J. V. Barth and K Kern, Modular Assembly of Two-Dimensional Metal-Organic Coordination Networks at a Metal Surface, *Angew. Chem., Int. Ed.* 2003, **42**, 2670-2673.

10 S. Stepanow, M. Lingenfelder, A. Dmitriev, H. Spillmann, E. Delvigne, N. Lin, X. Deng, C. Cai, J. V. Barth and K. Kern, Steering Molecular Organization and Host Guest Interactions Using Two-Dimensional Nanoporous Coordination Systems, *Nat. Mater.* 2004, **3**, 229-233.

11 H. Walch, J. Dienstmaier, G. Eder, R. Gutzler, S. Schlögl, T. Sirtl, K. Das, M. Schmittel and M. Lackinger, Extended Two-Dimensional Metal-Organic Frameworks Based on Thiolate-Copper Coordination Bonds, *J. Am. Chem. Soc.* 2011, **133**, 7009-7915.

12 Miao Yu, Wei Xu, N. Kalashnyk, Y. Benjalal, S. Nagarajan, F. Masini, E. Lægsgaard, M. Hliwa, X. Bouju, A. Gourdon, C. Joachim, F. Besenbacher and T. R. Linderoth, From Zero to Two Dimensions: Supramolecular Nanostructures Formed from Perylene-3,4,9,10-tetracarboxylic Diimide (PTCDI) and Ni on the Au(111) Surface Through the Interplay Between Hydrogen-Bonding and Electrostatic Metal-Organic Interactions, *Nano Res.* 2012, **5**, 903-916.

13 D. Heim, D. Écija, K. Seufert, W. Auwärter, C. Aurisicchio, C. Fabbro, D. Bonifazi and J. V. Barth, Self-Assembly of Flexible One- Dimensional Coordination Polymers on Metal Surfaces, *J. Am. Chem. Soc.* 2010, **132**, 6783-6790.

14 A. Saywell, W. Greń, G. Franc, A. Gourdon, X. Bouju and L. Grill, Manipulating the Conformation of Single Organometallic Chains on Au(111), *J. Phys. Chem. C* 2014, **118**, 1719-1728.

15 J. Hieulle, D. Peyrot, Z. Jiang and F. Silly, Engineering Two-Dimensional Hybrid NaCl-Organic Coordinated Nanoarchitectures on Metal Surface, *Chem. Commun.* 2015, **51**, 13162-13165.

16 J. Meyer, A. Nickel, R. Ohmann, Lokamani, C. Toher, D. A. Ryndyk, Y. Garmshausen, S. Hecht, F. Moresco and G. Cuniberti, Tuning the formation of discrete coordination nanostructures, *Chem. Commun.* 2015, **51**, 12621-12624.

17 L. Schüller, V. Haapasilta, S. Kuhn, H. Pinto, R. Bechstein, A. S. Foster and A. Kühnle, Deposition Order Controls the First Stages of a MetalâĹŠOrganic Coordination Network on an Insulator Surface, *J. Phys. Chem. C* 2016, **120**, 14730-14735.

18 M. Valiev, E. J. Bylaska, N. Govind, K. Kowalski, T. P. Straatsma, H. J. J. van Dam, D. Wang, J. Nieplocha, E. Apra, T. L. Windus and W. A. de Jong, NWChem: a comprehensive and scalable open-source solution for large scale molecular simulations, *Comput. Phys. Commun.* 2010, **181**, 1477-1489.

19 S. Grimme, Semiempirical GGA-type Density Functional Constructed With a Long-Range Dispersion Correction, *J. Comp. Chem.* 2006, **27**, 1787-1799.

20 M.-A. Dubois, X. Bouju and A. Rochefort, DyFlex, a highly parallel tool for dynamical STM imaging of large molecular systems, submitted, **2018**.

21 N. Boulanger-Lewandowski and A. Rochefort, Intrusive STM Imaging, *Phys. Rev. B* 2011, **83** 115430.

22 G. Landrum, YAeHMOP (Yet Another Extended Hückel Molecular Orbital Package); Cornell University: Ithaca, NY, 1995.

23 Y. J. Dappe, M. Andersen, R. Balog, L. Hornæker and X. Bouju, Adsorption and STM Imaging of Polycyclic Aromatic Hydrocarbons on Graphene, *Phys. Rev. B* 2015, **91**, 045427.

24 P. Sautet and C. Joachim, Electronic Transmission Coefficient for the Single-Impurity Problem in the Scattering-Matrix Approach, *Phys. Rev. B* 1988, **38**, 12238-12247.

25 S. L. Tait, A. Langner, N. Lin, R. Chandrasekar, O. Fuhr, M. Ruben and K. Kern, Assembling Isostructural Metal-Organic Coordination Architectures on Cu(100), Ag(100) and Ag(111) Substrates, *ChemPhysChem.* 2008, **9**, 2495-2499.

26 A. Langner, S. L. Tait, N. Lin, R. Chandrasekar, M. Ruben and

K. Kern, Ordering and Stabilization of Metal-Organic Coordination Chains by Hierarchical Assembly through Hydrogen Bonding at a Surface, *Angew. Chem. Int. Ed.* 2008, **47**, 8835-8838.

27 S. L. Tait, A. Langner, N. Lin, S. Stepanow, C. Rajadurai, M. Ruben and K. Kern, One-Dimensional Self-Assembled Molecular Chains on Cu(100): Interplay between Surface-Assisted Coordination Chemistry and Substrate Commensurability, *J. Phys. Chem. C* 2007, **111**, 10982-10987.

28 X. Zhang, N. Li, H. Wang, C. Yuan, G. Gu, Y. Zhang, D. Nieckarz, P. Szabelski, S. Hou, B. K. Teo and Y. Wang, Influence of Relativistic Effects on Assembled Structures of V-Shaped Bispyridine Molecules on M(111) Surfaces Where M = Cu, Ag, Au, *ACS Nano* 2017, **11**, 8511-8518.

29 M. Fujita, Y. J. Kwon, S. Washizu and K. Ogura, Preparation, Clathration Ability, and Catalysis of a Two-Dimensional Square Network Material Composed of Cadmium(II) and 4,4'-Bipyridine, *J. Am. Chem. Soc.* 1994, **116**, 1151-1152.

30 Y.-X. Diao, M.-J. Han, L.-J. Wan, K. Itaya, T. Uchida, H. Miyake, A. Yamakata and M. Osawa, Adsorbed Structures of 4,4'-Bipyridine on Cu(111) in Acid Studied by STM and IR, *Langmuir* 2006, **22**, 3640-3646.

31 Jascha Repp, Gerhard Meyer, Fredrik E. Olsson and Mats Persson, Controlling the Charge State of Individual Gold Adatoms, *Science* 2004, **305**, 493-495.

32 W. Steurer, J. Repp, L. Gross, I. Scivetti, M. Persson and G. Meyer, Manipulation of the Charge State of Single Au Atoms on Insulating Multilayer Films, *Phys. Rev. Lett.* 2015, **114**, 036801.